J. Fluid Mech. (2001), *vol.* 444, *pp.* 321–342. Printed in the United Kingdom

Stationary d.c. streaming due to shape oscillations of a droplet and its effect on mass transfer in liquid–liquid systems

By A. L. YARIN

Faculty of Mechanical Engineering, Technion – Israel Institute of Technology, Haifa 32000, Israel

(Received 15 June 2000 and in revised form 27 March 2001)

The work is devoted to stationary streaming flows resulting from standing capillary waves at interfaces between two immiscible liquids and their effect on the mass transfer rate of a passive scalar. In particular, oscillating liquid droplets immersed in another immiscible liquid are considered. Secondary streaming flows in the Stokes layers near the interface are calculated, as well as the corresponding vortical flows arising in the bulk. It is shown that the vortices can drastically enhance the mass transfer rate of a passive scalar which is to be extracted by one liquid from the other. The corresponding Sherwood number is of the order of $[|u_{int}|a/\mathscr{D}_1]^{1/2}$, where $|u_{int}|$ is the magnitude of the interfacial streaming velocity, a is the droplet radius, and $\mathscr{D}_1$ is the diffusion coefficient in liquid 1 (inside the droplet). This means that the effective diffusion coefficient is of the order of $\mathscr{D}_1[|u_{int}|a/\mathscr{D}_1]^{1/2}$, which is two orders of magnitude higher than $\mathscr{D}_1$. The results obtained show that such flows can be of potential interest for novel bioseparator devices.

1. Introduction

Various waves (including standing capillary waves) are capable of generating stationary d.c. streaming flows (cf. the seminal paper of Longuet-Higgins 1953, the monograph of Mei 1989, Chap. 9, and references therein). Dore (1970, 1972, 1973) extended the theory for planar two-layer systems (cf. §9 below). Such d.c. streaming flows are kindred to the well-known acoustic streaming first recognized by Rayleigh (1883, 1945). The streaming also arises when a cylinder or a sphere (solid, or a droplet, or bubble) oscillates in a fluid or gas at rest, or vice versa; an oscillatory motion of the medium is sustained about such bodies (cf. for example, Schlichting 1932, 1979, and a recent review of Riley (1997), where such flows are termed Type (*a*)). They can significantly affect the heat and mass transfer rate at the body surface (Davidson 1971, 1973; Gopinath & Mills 1993; Yarin *et al.* 1999; Kawahara *et al.* 2000; and references therein).

The streaming flows can, as we expect, create vortices near liquid–liquid interfaces and thus can be employed for enhancement of mass transfer in novel bioseparators. Similar ideas were put forward in studies of the effective diffusion arising in vortical flows in such contexts as fluid mixing in laminar flows, turbulent mixing in combustion, heat flow in a convecting plasma, etc. (Rosenbluth *et al.* 1987; Vold 1999; and references therein).

In a recent work Longuet–Higgins (1998) considered the streaming flows about a spherically symmetric bubble undergoing small lateral and radial oscillations simultaneously; shape oscillations were not accounted for. In the present work we consider

the streaming flow and the corresponding mass transfer effects generated by shape oscillations of a droplet/bubble immersed in a host immiscible liquid. In particular, we consider standing capillary waves at an interface between a droplet and an immiscible host liquid. Such monochromatic capillary waves on the droplet may be generated acoustically as in Trinh, Zwern & Wang (1982) and Trinh & Wang (1982). We demonstrate the appearance of stationary streaming flows. We then study their effect on mass transfer at the interface and show that it may be enhanced drastically by the streaming. This makes it possible to develop a new type of novel bioseparator which employs shape oscillations of droplets in emulsions.

In § 2 physical estimates of the effects involved are given. In § 3 we present the governing equations for the Stokes layers near the liquid–liquid interface with capillary waves. Inner streaming flows arising near the interface of an oscillating droplet are treated in § 4. The corresponding outer streaming in the bulk is considered in § 5. It is matched with the inner streaming in § 6, where the flow field of the stationary secondary flow arising inside and outside the droplet is discussed. The corresponding particular cases are illustrated in § 7. Mass transfer through the droplet interface is treated in § 8. Section 9 contains a summary and concluding remarks.

2. Physical estimates for capillary oscillations of liquid droplets in immiscible liquid–liquid systems

Standing ultrasonic waves are able to generate significant acoustic streaming flows in gases (Trinh & Robey 1994; Yarin *et al.* 1999). In the latter work it was shown that the streaming velocity in a gas is of the order of several $\mathrm{cm\,s^{-1}}$ for fields of about 160 to 165 dB. Assuming the amplitude of the standing wave in an ultrasonic acoustic levitator as $A_{0e} = 2 \times 10^4\,\mathrm{dyn\,cm^{-2}}$ (which corresponds to 160 dB under the definition of the sound pressure level, SPL, used in Yarin *et al.* 1999), the corresponding velocity scale in the sound wave

$$B = \frac{A_{0e}}{\rho_0 c_0} \tag{2.1}$$

for water is $B = 0.133\,\mathrm{cm\,s^{-1}}$. Here $\rho_0 = 1\,\mathrm{g\,cm^{-3}}$ is the unperturbed density and $c_0 = 15 \times 10^4\,\mathrm{cm\,s^{-1}}$ is the sound velocity in water. Assuming the angular frequency of the ultrasound wave as $\omega = 2\pi \times 56\,000\,\mathrm{Hz}$, and the droplet radius $a = 1\,\mathrm{cm}$ (we consider a droplet levitated in a liquid–liquid system), then the estimate of the steady streaming velocity (Yarin *et al.* 1999)

$$B_s = \frac{B^2}{\omega a} \tag{2.2}$$

is $B_s = 0.5 \times 10^{-7}\,\mathrm{cm\,s^{-1}}$. This estimate shows that it is practically impossible to generate significant acoustic streaming flows in a liquid–liquid systems even with recourse to acoustic levitators with high SPL values.

However, significant stationary streaming flows in liquid–liquid systems can be generated by capillary waves. Consider a drop of liquid 1 levitated in an immiscible liquid 2 and undergoing small forced capillary oscillations (cf. figure 1), which can be imposed, for example, by an acoustic field with modulated amplitude like in Trinh *et al.* (1982) and Trinh & Wang (1982). The droplet volume-equivalent radius is denoted by a, the densities and (low) viscosities of the liquids by ρ_1 and ρ_2, and μ_1 and μ_2, respectively, and the interfacial tension by σ. Buoyancy effects are neglected or

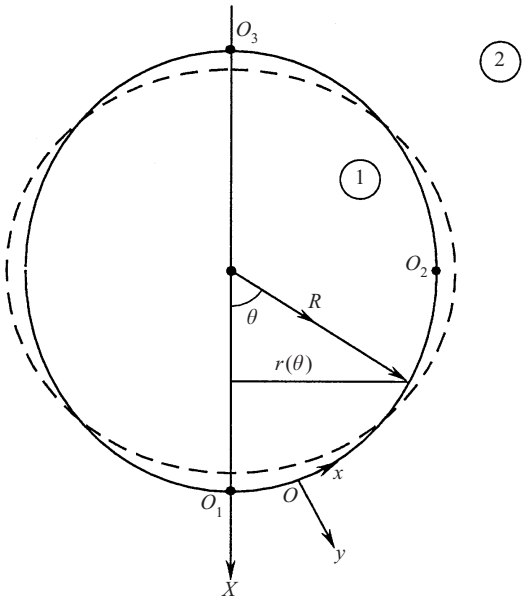

FIGURE 1. Sketch of forced capillary oscillations of liquid droplet 1 immersed in an immiscible liquid 2.

compensated by the acoustic levitation force. We consider here only axisymmetric modes. The frequency of the imposed oscillations is assumed to be close to one of the eigenfrequencies (Lamb 1959, § 275)

$$\omega = \left\{ \frac{n(n+1)(n-1)(n+2)}{[\rho_1(n+1)+\rho_2 n]} \cdot \frac{\sigma}{a^3} \right\}^{1/2}, \tag{2.3}$$

where n is the wavenumber.

Take the droplet volume as $1.5\,\mathrm{cm}^3$, which corresponds to $a = 0.71\,\mathrm{cm}$, $\rho_1 = 1\,\mathrm{g\,cm^{-3}}$, $\rho_2 = 0.9\,\mathrm{g\,cm^{-3}}$, $\sigma = 70\,\mathrm{g\,s^{-2}}$. For $n = 2$ we obtain from (2.3) $\omega = 31.3\,\mathrm{s^{-1}}$, and for $n = 3$, $\omega = 59.19\,\mathrm{s^{-1}}$. The inviscid solution for droplet oscillations of small amplitude yields the following velocity components tangent to the interface in liquids 1 and 2:

$$U_{*i} = B_i \sin \omega t \frac{\mathrm{d}}{\mathrm{d}\theta}[P_n(\cos\theta)], \tag{2.4}$$

where P_n is a Legendre polynomial. Here and hereinafter subscripts $i = 1$ and 2 correspond to liquids 1 (inside the droplet; cf. figure 1) and 2 (outside), respectively. The velocity amplitudes are given by

$$B_1 = -\frac{(a\zeta_{0n})\omega}{n}, \quad B_2 = \frac{(a\zeta_{0n})\omega}{n+1}, \tag{2.5a,b}$$

where $a\zeta_{0n}$ is the oscillation amplitude ($\zeta_{0n} \ll 1$). We take for the estimation $\omega = (31.3 + 59.19)/2 = 45.25\,\mathrm{s^{-1}}$ and $a\zeta_{0n} = 0.071\,\mathrm{cm}$. For the modes $n = 2$ and $n = 3$ we obtain the average denominators in (2.5) as 2.5, whence from (2.5) $|B_i| = 1.29\,\mathrm{cm\,s^{-1}}$. This is the velocity magnitude of the primary flow due to the capillary oscillations of the droplet.

The corresponding steady streaming velocity is expected to be of the order of

$$B_s \simeq \frac{B_i^2}{\omega a}. \tag{2.6}$$

For $\omega \sim 45.25\,\mathrm{s}^{-1}$ and $a = 0.71\,\mathrm{cm}$, (2.6) yields $B_s = 0.052\,\mathrm{cm\,s}^{-1}$.

The following simplifications were used to arrive at (2.4): (i) viscous effects in the bulk were neglected, (ii) terms $\Delta U_i = O(B_i\varepsilon)$, $\varepsilon \sim \zeta_{0n} \ll 1$ were omitted, since the boundary conditions at the wave interface have been projected onto the unperturbed interface, and (iii) the geometrical factors in the boundary conditions at the interface were linearized assuming small angles of inclination, which means that terms $O(B_i\varepsilon^2)$ were neglected. The terms ΔU_i will be considered in more detail in § 4, where we show that they do not affect the stationary streaming arising due to the primary capillary wave, whereas the terms $O(B_i\varepsilon^2)$ do not affect the stationary streaming due to their smallness.

Viscous effects in the bulk can be neglected for Reynolds numbers (Levich 1962)

$$Re = \frac{\omega a^2}{\nu_1} \gg 1. \tag{2.7}$$

Taking the kinematic viscosity of liquid 1 as $\nu_1 = 0.032\,\mathrm{cm^2\,s^{-1}}$, we obtain $Re = 713$, and the inequality (2.7) is satisfied, which supports *a posteriori* recourse to the inviscid solution for the primary flow in the bulk. However, for $Re \gg 1$ near the interface Stokes layers should exist (boundary layers), where steady d.c. streaming is developed. The thickness of these layers is estimated to be of the order of

$$\delta = \left(\frac{\nu}{\omega}\right)^{1/2}, \tag{2.8}$$

which yields for $\nu_i = 0.032\,\mathrm{cm^2\,s^{-1}}$ and $\omega \sim 45.25\,\mathrm{s}^{-1}$ the value of $\delta = 0.027\,\mathrm{cm} \ll a = 0.71\,\mathrm{cm}$.

The reciprocal Strouhal number

$$S^{-1} = \frac{|B_i|}{\omega a} \sim \varepsilon \tag{2.9}$$

is estimated using the following values: $|B_i| = 1.29\,\mathrm{cm\,s}^{-1}$, $\omega = 45.25\,\mathrm{s}^{-1}$ and $a = 0.71\,\mathrm{cm}$, which yields $S^{-1} = 0.04$. This value is sufficiently small compared to unity to permit application of the method of successive approximations for calculating the d.c. streaming flow (Schlichting 1932, 1979; Yarin *et al.* 1999).

3. The governing equations for the Stokes layers near the interface

In considering the Stokes layers at the beginning of this section, we dispense for the moment with the subscripts corresponding to liquids 1 and 2, since we are dealing with both of them simultaneously. The equations describing the flow in the Stokes layers near the interface, where the viscous effects are important, are written as

$$\frac{\partial ur}{\partial x} + \frac{\partial vr}{\partial y} = 0, \tag{3.1a}$$

$$\frac{\partial u}{\partial t} + u\frac{\partial u}{\partial x} + v\frac{\partial u}{\partial y} = \frac{\partial U}{\partial t} + U\frac{\partial U}{\partial x} + \nu\frac{\partial^2 u}{\partial y^2} \tag{3.1b}$$

(cf. Schlichting 1979).

For the Stokes layers near the interface, coordinates x and y are taken along the perturbed interface and normal to it, respectively. Replacing the scheme by that of figure 1 (the x-coordinate taken along the unperturbed interface), the difference is of $O(\varepsilon^2)$, which we neglect throughout the following analysis and use x accordingly. Coordinate y is negative in liquid 1 and positive in liquid 2, its zero corresponding to a perturbed interface. Also $r(x)$ is the cross-sectional radius of the droplet, $r = a\sin(x/a)$. The velocity components u and v refer to x and y respectively. The velocity at the outer boundary of the Stokes layers U is given by

$$U = U_* + \Delta U, \tag{3.2}$$

where $U_* = O(B)$ is given by (2.4) and ΔU is its correction of $O(\varepsilon B_i)$ mentioned in § 2. Equations (3.1a, b) are referred to the axes moving with the perturbed interface. The fact that the continuity equation (3.1a) has the same form as that with y measured from the interface at rest is proved in Lamb (1952, p. 12). Equation (3.1b) is discussed at the end of the present section.

In our treatment we render the velocity components u, U, U_* and ΔU dimensionless by the velocity scale B, v by $B\delta/a$, x and r by a, y by δ, and t by ω^{-1}. The governing equations (3.1) and (3.2) become

$$\frac{\partial \bar{u}\bar{r}}{\partial \bar{x}} + \frac{\partial \bar{v}\bar{r}}{\partial \bar{y}} = 0, \tag{3.3a}$$

$$\frac{\partial \bar{u}}{\partial \bar{t}} + \varepsilon\left(\bar{u}\frac{\partial \bar{u}}{\partial \bar{x}} + \bar{v}\frac{\partial \bar{u}}{\partial \bar{y}}\right) = \frac{\partial \bar{U}_*}{\partial \bar{t}} + \frac{\partial^2 \bar{u}}{\partial \bar{y}^2} + \varepsilon\left(\bar{U}_*\frac{\partial \bar{U}_*}{\partial \bar{x}} + \frac{\partial \Delta\bar{U}}{\partial \bar{t}}\right), \tag{3.3b}$$

where dimensionless variables are denoted by overbars.

By virtue of the smallness of the parameter ε, we resort to the asymptotic expansions

$$\bar{u} = \bar{u}^{(0)}(\bar{x}, \bar{y}, \bar{t}) + \varepsilon\bar{u}^{(1)}(\bar{x}, \bar{y}, t) + \cdots, \quad \bar{v} = \bar{v}^{(0)}(\bar{x}, \bar{y}, \bar{t}) + \varepsilon\bar{v}^{(1)}(\bar{x}, \bar{y}, \bar{t}) + \cdots, \tag{3.4a, b}$$

$$\bar{u}^{(0)}, \bar{v}^{(0)}, \bar{u}^{(1)}, \bar{v}^{(1)} = O(1). \tag{3.4c}$$

Here and hereinafter superscripts 0 and 1 are used to distinguish between the leading-order and perturbation velocities. Substituting (3.4) in (3.3), we obtain at the leading order $O(1)$ the following equations:

$$\frac{\partial u^{(0)}r}{\partial x} + \frac{\partial v^{(0)}r}{\partial y} = 0, \tag{3.5a}$$

$$\frac{\partial u^{(0)}}{\partial t} = \nu\frac{\partial^2 u^{(0)}}{\partial y^2} + \frac{\partial U_*}{\partial t}. \tag{3.5b}$$

The next order, $O(\varepsilon)$, yields

$$\frac{\partial u^{(1)}r}{\partial x} + \frac{\partial v^{(1)}r}{\partial y} = 0, \tag{3.6a}$$

$$\frac{\partial u^{(1)}}{\partial t} = \nu\frac{\partial^2 u^{(1)}}{\partial y^2} - \left[u^{(0)}\frac{\partial u^{(0)}}{\partial x} + v^{(0)}\frac{\partial u^{(0)}}{\partial y}\right] + U_*\frac{\partial U*}{\partial x} + \frac{\partial \Delta U}{\partial t}. \tag{3.6b}$$

Terms $O(\varepsilon^2)$ and smaller are not considered. Equations (3.5) and (3.6) are presented in the dimensional form for convenience; $u^{(0)} = B\bar{u}^{(0)}$, $v^{(0)} = (B\delta/a)\bar{v}^{(0)}$, $u^{(1)} = \varepsilon B\bar{u}^{(1)}$, and $v^{(1)} = \varepsilon(B\delta/a)\bar{v}^{(1)}$.

It is emphasized that in the present problem a moving coordinate system is needed because the amplitude of the surface oscillations $a\zeta_{0n}$ may be comparable to the

Stokes boundary layer thickness δ (cf. the values presented in § 2). It is easy to show that because the oscillations are small compared to the droplet radius, both rotation and translation of the interface are small. In the present axisymmetric case spherical radial and angular coordinates r and θ are replaced by $y = r - a[1 + \zeta(\theta, t)]$ and θ, where the surface perturbation $\zeta = O(\zeta_{0n}) = O(\varepsilon)$. The spatial derivatives $\partial/\partial r$ and $\partial/\partial\theta$ are replaced by $\partial/\partial y$ and $\partial/\partial\theta - a(\partial\zeta/\partial\theta)\,\partial/\partial y$, respectively, and the time derivative by $\partial/\partial t - a(\partial\zeta/\partial t)\,\partial/\partial y$; also $\partial/\partial x = a^{-1}\partial/\partial\theta$. The velocity relative to the moving coordinate system is also introduced. It is easy to see that in the boundary layer the leading terms in the θ-projection of the momentum equation are those in (3.1b) and (3.3b). The largest additional terms would be of $O(\varepsilon^2)$ in (3.3b). Such terms are not considered in the present asymptotic analysis, as discussed above.

4. Streaming flows inside and outside a droplet undergoing forced capillary oscillations

The solutions of equations (3.5) should match with the inviscid flows given by (2.4) away from the interface, and guarantee continuity of the velocity and shear stress at the interface, as well as impenetrability of the interface. Accordingly they satisfy the following boundary conditions:

$$u_1^{(0)} = B_1 \sin(\omega t)\tilde{U}(x) \quad \text{as} \quad \eta \to -\infty, \tag{4.1a}$$

$$u_2^{(0)} = B_2 \sin(\omega t)\tilde{U}(x) \quad \text{as} \quad \eta \to +\infty, \tag{4.1b}$$

$$y = 0, \quad u_1^{(0)} = u_2^{(0)}, \tag{4.1c}$$

$$y = 0, \quad \mu_1 \frac{\partial u_1^{(0)}}{\partial y} = \mu_2 \frac{\partial u_2^{(0)}}{\partial y}, \tag{4.1d}$$

$$y = 0, \quad v_1^{(0)} = v_2^{(0)} = 0, \tag{4.1e,f}$$

where

$$\tilde{U}(x) = \frac{\mathrm{d}}{\mathrm{d}\theta}[P_n(\cos\theta)], \quad \theta = \frac{x}{a}, \tag{4.2a,b}$$

and $\eta(y)$ is given below in (4.4a). The jump in the normal stresses at the interface $y = 0$ should be in balance with the capillary pressure associated with an additional deformation of the interface. It is discussed at the end of the present section.

The solution of equations (3.5) subject to the boundary conditions (4.1) is as follows:

$$u_i^{(0)} = \tilde{U}(x)[B_i \sin\omega t + m_i E_i \,\mathrm{e}^{m_i\eta} \sin(\omega t + m_i\eta)], \tag{4.3a}$$

$$v_i^{(0)} = -\sqrt{\frac{2\nu_i}{\omega}}\left(\frac{\mathrm{d}\tilde{U}}{\mathrm{d}x} + \frac{\tilde{U}}{r}\frac{\mathrm{d}r}{\mathrm{d}x}\right)[B_i\eta \sin\omega t + \tfrac{1}{2}E_i \sin\omega t\,\mathrm{e}^{m_i\eta}(\cos m_i\eta + \sin m_i\eta)$$
$$+\tfrac{1}{2}E_i \cos\omega t\,\mathrm{e}^{m_i\eta}(\sin m_i\eta - \cos m_i\eta) - \tfrac{1}{2}E_i \sin\omega t + \tfrac{1}{2}E_i \cos\omega t], \tag{4.3b}$$

where

$$\eta = y\sqrt{\frac{\omega}{2\nu_i}}, \tag{4.4a}$$

$$m_i = \begin{cases} +1 \ (i = 1 \text{ in liquid 1, where } \eta < 0) \\ -1 \ (i = 2 \text{ in liquid 2, where } \eta > 0), \end{cases} \tag{4.4b}$$

$$E_1 = \frac{B_2 - B_1}{1 + (\mu_1\rho_1/\mu_2\rho_2)^{1/2}}, \quad E_2 = \frac{B_2 - B_1}{1 + (\mu_2\rho_2/\mu_1\rho_1)^{1/2}}; \tag{4.4c,d}$$

x is the arc length of the interface generatrix reckoned from the droplet bottom O_1 (see figure 1).

At the next order of magnitude we seek to find a stationary streaming $\langle u_i^{(1)}\rangle$ and $\langle v_i^{(1)}\rangle$, with the averaging carried out over multiple cycles of the primary capillary wave. Since $\langle \partial u_i^{(1)}/\partial t\rangle = 0$, equations (3.6) reduce to

$$\frac{\partial\langle u_i^{(1)}\rangle r}{\partial x} + \frac{\partial\langle v_i^{(1)}\rangle r}{\partial y} = 0, \tag{4.5a}$$

$$\frac{\partial^2\langle u_i^{(1)}\rangle}{\partial\eta^2} = \frac{2}{\omega}\left\langle u_i^{(0)}\frac{\partial u_i^{(0)}}{\partial x} + v_i^{(0)}\frac{\partial u_i^{(0)}}{\partial y} - U_{*i}\frac{\partial U_{*i}}{\partial x} - \frac{\partial\Delta U_i}{\partial t}\right\rangle. \tag{4.5b}$$

From the solution for the inviscid potential flow due to capillary waves, leading to the characteristic equation (2.3), it is readily seen that the time dependence of ΔU_i is given by $\Delta U_i \sim \sin\omega t$. Therefore $\langle\partial\Delta U_i/\partial t\rangle = 0$. Note that the time averaging we are dealing with here and hereinafter means that

$$\langle\cos^2\omega t\rangle = \langle\sin^2\omega t\rangle = \tfrac{1}{2}, \quad \langle\sin\omega t\cos\omega t\rangle = 0. \tag{4.6a–c}$$

Substituting (2.4) and (4.3) in (4.5) and integrating, we obtain near the interface

$$\begin{aligned}\langle u_i^{(1)}\rangle = {} & \frac{1}{\omega}\tilde{U}\frac{\mathrm{d}\tilde{U}}{\mathrm{d}x}\left(\frac{E_i^2}{4}\,\mathrm{e}^{2m_i\eta} + B_iE_im_i\,\mathrm{e}^{m_i\eta}\sin m_i\eta\right)\\ & -\frac{E_i}{\omega}\left(\tilde{U}\frac{\mathrm{d}\tilde{U}}{\mathrm{d}x} + \frac{\tilde{U}^2}{r}\frac{\mathrm{d}r}{\mathrm{d}x}\right)\left[\frac{B_i}{2}\eta\,\mathrm{e}^{m_i\eta}(\cos m_i\eta + \sin m_i\eta)\right.\\ & \left. -B_im_i\,\mathrm{e}^{m_i\eta}\sin m_i\eta - \tfrac{1}{2}E_i\,\mathrm{e}^{m_i\eta}\cos m_i\eta\right] + \beta_i(x)\eta + \alpha_i(x),\end{aligned} \tag{4.7a}$$

$$\begin{aligned}\langle v_i^{(1)}\rangle = {} & -\sqrt{\frac{2\nu_i}{\omega}}\left\{\left[\frac{\mathrm{d}}{\mathrm{d}x}\left(\tilde{U}\frac{\mathrm{d}\tilde{U}}{\mathrm{d}x}\right) + \frac{1}{r}\frac{\mathrm{d}r}{\mathrm{d}x}\tilde{U}\frac{\mathrm{d}\tilde{U}}{\mathrm{d}x}\right]\frac{1}{\omega}\right.\\ & \times\left[\frac{E_i^2}{8m_i}\,\mathrm{e}^{2m_i\eta} + \frac{B_iE_i}{2}\,\mathrm{e}^{m_i\eta}(\sin m_i\eta - \cos m_i\eta) - \frac{E_i^2}{8m_i} + \frac{B_iE_i}{2}\right]\\ & -\left[\frac{\mathrm{d}}{\mathrm{d}x}\left(\tilde{U}\frac{\mathrm{d}\tilde{U}}{\mathrm{d}x} + \frac{\tilde{U}^2}{r}\frac{\mathrm{d}r}{\mathrm{d}x}\right) + \frac{1}{r}\frac{\mathrm{d}r}{\mathrm{d}x}\left(\tilde{U}\frac{\mathrm{d}\tilde{U}}{\mathrm{d}x} + \frac{\tilde{U}^2}{r}\frac{\mathrm{d}r}{\mathrm{d}x}\right)\right]\\ & \times\frac{E_i}{\omega}\left[\frac{B_im_i}{2}\eta\,\mathrm{e}^{m_i\eta}\sin m_i\eta - \frac{3B_i}{4}\,\mathrm{e}^{m_i\eta}(\sin m_i\eta - \cos m_i\eta)\right.\\ & \left.\left. -\frac{E_im_i}{4}\,\mathrm{e}^{m_i\eta}(\cos m_i\eta + \sin m_i\eta) - \frac{3B_i}{4} + \frac{E_im_i}{4}\right]\right.\\ & \left. +\left(\frac{\mathrm{d}\beta_i}{\mathrm{d}x} + \frac{1}{r}\frac{\mathrm{d}r}{\mathrm{d}x}\beta_i\right)\frac{\eta^2}{2} + \left(\frac{\mathrm{d}\alpha_i}{\mathrm{d}x} + \frac{1}{r}\frac{\mathrm{d}r}{\mathrm{d}x}\alpha_i\right)\eta\right\}.\end{aligned} \tag{4.7b}$$

We subject the flow component $\langle v_i^{(1)}\rangle$ to the boundary condition $\langle v_i^{(1)}\rangle = 0$ at $\eta = 0$. Functions $\alpha_i(x)$ and $\beta_i(x)$ resulted from integration in η. They will be found later on when matching the inner streaming in the Stokes layers at the interface with the

outer streaming flow in the bulk. For this matching the following limiting expressions obtained from (4.7) will be used:

$$\frac{\partial\langle u_i^{(1)}\rangle}{\partial\eta} = \frac{1}{\omega}\tilde{U}\frac{\mathrm{d}\tilde{U}}{\mathrm{d}x}\left(\frac{E_i^2}{2}m_i + B_iE_i\right) + \frac{E_i}{\omega}\left(\tilde{U}\frac{\mathrm{d}\tilde{U}}{\mathrm{d}x} + \frac{\tilde{U}^2}{r}\frac{\mathrm{d}r}{\mathrm{d}x}\right)\left(\frac{B_i}{2} + \frac{E_im_i}{2}\right) + \beta_i \quad \text{at} \quad \eta = 0, \tag{4.8a}$$

$$\langle u_i^{(1)}\rangle = \tilde{U}\frac{\mathrm{d}\tilde{U}}{\mathrm{d}x}\frac{E_i^2}{4\omega} + \left(\tilde{U}\frac{\mathrm{d}\tilde{U}}{\mathrm{d}x} + \frac{\tilde{U}^2}{r}\frac{\mathrm{d}r}{\mathrm{d}x}\right)\frac{E_i^2}{2\omega} + \alpha_i \quad \text{at} \quad \eta = 0. \tag{4.8b}$$

The balance of the normal stresses at the interface $y = 0$ allows us to estimate *a posteriori* an additional deformation of the interface due to the flow in the boundary layers near it. Variation of the interface curvature relative to that of the inviscid problem $\overline{\Delta K}$ may be estimated from the above balance and the solutions (4.3) and (4.7). Using (4.3), we obtain $\overline{\Delta K} \sim \mu_i B_i/\sigma$. Since $\mu_i \sim 10^{-2}\,\mathrm{g\,cm^{-1}\,s^{-1}}$, $B_i \sim 1\,\mathrm{cm\,s^{-1}}$ and $\sigma \sim 10^2\,\mathrm{g\,s^{-2}}$ we obtain $\overline{\Delta K} \sim 10^{-4}$. Given the value of $\varepsilon = 0.04$ obtained from (2.9), we see that $\mu_i B_i/\sigma \sim \varepsilon^2$, and $\langle\overline{\Delta K}\rangle \sim \varepsilon^2$ due to the flow given by (4.3). Similarly due to the flow given by (4.7), $\langle\overline{\Delta K}\rangle \sim \varepsilon^3$. In both cases the variation of the interface shape due to the flows in the Stokes layers near the interface is negligibly small, as was assumed. It is seen from (4.7) and (4.8) that the magnitude of the inner streaming velocity is $B_i^2/(\omega a)$, as was assumed in (2.6).

5. Outer streaming

We now estimate the Reynolds number Re_s of the outer streaming in the bulk entrained by the inner streaming. For $B_s = 0.052\,\mathrm{cm\,s^{-1}}$ (cf. § 2), $a = 0.71\,\mathrm{cm}$ and $\nu_i \simeq 0.032\,\mathrm{cm^2\,s^{-1}}$, we find

$$Re_s = \frac{B_s a}{\nu_i} = 1.15. \tag{5.1}$$

A similar value of Re_s corresponds to the outer streaming flow inside an acoustically levitated droplet, which is driven by the acoustic streaming in gas in the situation studied by Yarin *et al.* (1999). There it was shown that the creeping flow approximation represents quite accurately the flow structure found experimentally in spite of the fact that at $Re_s \sim 1$ the inertial forces begin to play some role. In the present case the creeping flow solution may also be used as a first approximation of the outer streaming. Note also that Re_s decreases with the droplet radius as $a^{1/2}$.

The general solution of the Stokes equations for the creeping flow in spherical harmonics is given in Lamb (1959, §§ 335 and 336). When it is applied in the case of an almost spherical droplet with the only non-zero velocity component $v_\theta^{(i)}$ at the interface (the angular component), it can be shown (see Yarin *et al.* 1999) that the harmonics $\chi_m \equiv 0$ (in Lamb's 1959 notation).

We consider here only the flow corresponding to mode $n = 2$ of the oscillations, when due to (4.2)

$$\tilde{U}\frac{\mathrm{d}\tilde{U}}{\mathrm{d}x} = \frac{9}{a}(2\sin\theta\cos^3\theta - \sin\theta\cos\theta), \tag{5.2a}$$

$$\tilde{U}\frac{\mathrm{d}\tilde{U}}{\mathrm{d}x} + \frac{\tilde{U}^2}{r}\frac{\mathrm{d}r}{\mathrm{d}x} = \frac{9}{a}(3\sin\theta\cos^3\theta - \sin\theta\cos\theta). \tag{5.2b}$$

Here θ is the angular spherical coordinate (with $\theta = 0$ corresponding to the droplet bottom, see figure 1).

Bearing in mind that the outer streaming flow should be matched with the inner flow (4.7), (4.8) and bearing in mind (5.2), we see easily that the outer streaming inside the droplet subject to the condition of finiteness at $R = 0$ is described by the Lamb's solution (equations (8)–(11) and (15), pp. 596–597) with only four spherical harmonics p_2, φ_2, p_4 and φ_4:

$$\begin{pmatrix} p_2 \\ \varphi_2 \end{pmatrix} = \begin{pmatrix} A_1 \\ \gamma_1 \end{pmatrix} \frac{1}{2}(3X^2 - R^2), \tag{5.3a}$$

$$\begin{pmatrix} p_4 \\ \varphi_4 \end{pmatrix} = \begin{pmatrix} C_1 \\ D_1 \end{pmatrix} \frac{1}{8}(35X^4 - 30X^2R^2 + 3R^4), \tag{5.3b}$$

where the coefficients A_1, γ_1, C_1 and D_1 should be found via matching of the outer and inner streaming. We denote by p_m a solid harmonic of degree m and by φ_m an arbitrary harmonic of degree m, using a notation similar to that of Lamb (1959). Also X is the Cartesian coordinate associated with the droplet centre (with the X-axis spanning the droplet bottom and top, O_1 and O_3, in figure 1), and R is the radial spherical coordinate.

The outer streaming outside the droplet subject to the condition of finiteness at $R = \infty$ is described by Lamb's solution, again with only four spherical harmonics:

$$\begin{pmatrix} p_{-3} \\ \varphi_{-3} \end{pmatrix} = \begin{pmatrix} A_2 \\ \gamma_2 \end{pmatrix} \frac{1}{2}(3X^2 - R^2)\frac{1}{R^5}, \tag{5.4a}$$

$$\begin{pmatrix} p_{-5} \\ \varphi_{-5} \end{pmatrix} = \begin{pmatrix} C_2 \\ D_2 \end{pmatrix} \frac{1}{8}(35X^4 - 30X^2R^2 + 3R^4)\frac{1}{R^9}, \tag{5.4b}$$

where the coefficients A_2, γ_2, C_2, and D_2 also to be found via matching of the outer and inner streaming.

It is emphasized that the Lamb's solution yields velocity components in Cartesian coordinates. A simple transformation should be used to obtain from it the velocity components in spherical coordinates $v_{R,i}$ and $v_{\theta,i}$, as well as the stress $\sigma_{R\theta,i}$ used below (cf. Yarin *et al.* 1999).

6. Matching of the inner and outer streaming inside and outside the droplet

Matching of the inner and outer streaming flows in liquid 1 near the interface is achieved using the following boundary conditions for the tangential velocity and shear stress:

$$R = a - 0 \quad (y = -0,\ \eta \to -\infty), \quad \langle u_1^{(1)} \rangle = v_{\theta,1}, \tag{6.1a}$$

$$R = a - 0 \quad (y = -0,\ \eta \to -\infty), \quad \mu_1 \frac{\partial \langle u_1^{(1)} \rangle}{\partial y} = \sigma_{R\theta,1}. \tag{6.1b}$$

From the outer solution it is easy to show that $v_{R,1}|_{R=a-0} = 0$ as it also should be for the matching.

For matching in liquid 2 near the interface the following boundary conditions should be satisfied by the tangential velocity and shear stress:

$$R = a + 0 \quad (y = +0, \eta \to +\infty), \quad \langle u_2^{(1)} \rangle = v_{\theta,2}, \tag{6.2a}$$

$$R = a + 0 \quad (y = +0, \eta \to +\infty), \quad \mu_2 \frac{\partial \langle u_2^{(1)} \rangle}{\partial y} = \sigma_{R\theta,2}. \tag{6.2b}$$

The radial velocity component $v_{R,2}$ cancels out automatically at $R = a+0$, as it should for the matching.

We continue to discuss the case $n = 2$. Here, bearing in mind expressions (5.2), we present the streaming velocity at the outer boundary of the Stokes layers α_i, as well as β_i in the following form:

$$\alpha_i = \alpha_{i1}(2\sin\theta\cos^3\theta - \sin\theta\cos\theta) + \alpha_{i2}(3\sin\theta\cos^3\theta - \sin\theta\cos\theta), \tag{6.3a}$$

$$\beta_i = \beta_{i1}(2\sin\theta\cos^3\theta - \sin\theta\cos\theta) + \beta_{i2}(3\sin\theta\cos^3\theta - \sin\theta\cos\theta). \tag{6.3b}$$

Substituting (4.7a), (6.3), and the expressions for $v_{\theta,1}$ and $\sigma_{R\theta,1}$ based on (5.3) in the conditions (6.1), and using expression (9) of Lamb (1959, p. 596) at $R = a$, we obtain expressions for the coefficients of the spherical harmonics in liquid 1 A_1, γ_1, C_1, D_1 via α_{11}, α_{12}, which also yields relations between β_{11}, β_{12}, and α_{11}, α_{12}. Additionally, using (4.7a), (6.3), the expressions for $v_{\theta,2}$ and $\sigma_{R\theta,2}$ based on (5.4), as well as equation (9) of Lamb (1959, p. 596) at $R = a$, we obtain from the conditions (6.2) expressions for the coefficients of the spherical harmonics in liquid 2 A_2, γ_2, C_2, D_2 via α_{21}, α_{22}, which also yields relations between β_{21}, β_{22}, and α_{21}, α_{22}.

For matching of the inner streaming flows in the Stokes layers (4.7) at the interface, we pose the following conditions:

$$\eta = 0, \quad \langle u_1^{(1)}\rangle = \langle u_2^{(1)}\rangle, \tag{6.4a}$$

$$\eta = 0, \quad \mu_1 \tfrac{\partial\langle u_1^{(1)}\rangle}{\partial y} = \mu_2 \tfrac{\partial\langle u_2^{(1)}\rangle}{\partial y}. \tag{6.4b}$$

From these, using also (4.8a, b) and the relations between β_{11}, β_{12} and α_{11}, α_{12}, as well as between β_{21}, β_{22} and α_{21}, α_{22}, we arrive at a set of four equations for the four unknowns α_{11}, α_{12}, α_{21}, and α_{22}:

$$\alpha_{11} = \frac{9}{4\omega a}(E_2^2 - E_1^2) + \alpha_{21}, \tag{6.5a}$$

$$\alpha_{22} = \frac{9}{2\omega a}(E_1^2 - E_2^2) + \alpha_{12}, \tag{6.5b}$$

$$\mu_1(51\alpha_{11} + 24\alpha_{12}) + \mu_2(51\alpha_{21} + 24\alpha_{22}) = 63\left[\sqrt{\frac{\mu_2\rho_2}{2\omega}}\left(-\frac{E_2^2}{2} + B_2E_2\right) - \sqrt{\frac{\mu_1\rho_1}{2\omega}}\left(\frac{E_1^2}{2} + B_1E_1\right)\right], \tag{6.5c}$$

$$\mu_1(8\alpha_{11} + 47\alpha_{12}) + \mu_2(8\alpha_{21} + 47\alpha_{22}) = 63\left[\sqrt{\frac{\mu_2\rho_2}{2\omega}}\frac{E_2}{2}(B_2 - E_2) - \sqrt{\frac{\mu_1\rho_1}{2\omega}}\frac{E_1}{2}(B_1 + E_1)\right]. \tag{6.5d}$$

Solving equations (6.5) and rendering the velocities u_{int}, u'_{int}, u''_{int}, α_{11}, α_{12}, α_{21} and α_{22} dimensionless by the velocity scale of the streaming flow $B_1^2/\omega a$ (cf. (2.6)) with B_1 given by (2.5a), we arrive at the following expression to calculate the interfacial velocity $\bar{u}_{int}$ (overbars denote dimensionless parameters):

$$\overline{u_{int}} = \overline{u'_{int}}(2\sin\theta\cos^3\theta - \sin\theta\cos\theta) + \overline{u''_{int}}(3\sin\theta\cos^3\theta - \sin\theta\cos\theta), \tag{6.6}$$

where

$$\overline{u'_{int}} = \tfrac{9}{4}\bar{E}_1^2 + \bar{\alpha}_{11}, \quad \overline{u''_{int}} = \tfrac{9}{2}\bar{E}_1^2 + \bar{\alpha}_{12}, \tag{6.7a, b}$$

$$\bar{B}_2 = -\tfrac{2}{3}, \quad \bar{E}_1 = \frac{\bar{B}_2 - 1}{1 + (\mu_1\rho_1/\mu_2\rho_2)^{1/2}}, \quad \bar{E}_2 = \frac{\bar{B}_2 - 1}{1 + (\mu_2\rho_2/\mu_1\rho_1)^{1/2}}, \tag{6.7c–e}$$

$$K' = \frac{63}{1+\mu_2/\mu_1}\left(\frac{\rho_1\omega a^2}{2\mu_1}\right)^{1/2}\left[\left(\frac{\mu_2\rho_2}{\mu_1\rho_1}\right)^{1/2}\left(-\frac{\bar{E}_2^2}{2} + \bar{B}_2\bar{E}_2\right) - \left(\frac{\bar{E}_1^2}{2} + \bar{E}_1\right)\right]$$
$$-\frac{459}{4(1+\mu_2/\mu_1)}(\bar{E}_2^2 - \bar{E}_1^2) - \frac{108\mu_2/\mu_1}{1+\mu_2/\mu_1}(\bar{E}_1^2 - \bar{E}_2^2), \tag{6.7f}$$

$$K'' = \frac{63}{1+\mu_2/\mu_1}\left(\frac{\rho_1\omega a^2}{2\mu_1}\right)^{1/2}\left[\left(\frac{\mu_2\rho_2}{\mu_1\rho_1}\right)^{1/2}\frac{\bar{E}_2}{2}(\bar{B}_2 - \bar{E}_2) - \frac{\bar{E}_1}{2}(1 + \bar{E}_1)\right]$$
$$-\frac{18}{1+\mu_2/\mu_1}(\bar{E}_2^2 - \bar{E}_1^2) - \frac{423\mu_2/\mu_1}{2(1+\mu_2/\mu_1)}(\bar{E}_1^2 - \bar{E}_2^2), \tag{6.7g}$$

$$\left.\begin{aligned} \bar{\alpha}_{21} &= \frac{47K' - 24K''}{2205}, \quad \bar{\alpha}_{12} = \frac{51K'' - 8K'}{2205}, \\ \bar{\alpha}_{11} &= \tfrac{9}{4}(\bar{E}_2^2 - \bar{E}_1^2) + \bar{\alpha}_{21}, \quad \bar{\alpha}_{22} = \tfrac{9}{2}(\bar{E}_1^2 - \bar{E}_2^2) + \bar{\alpha}_{12}. \end{aligned}\right\} \tag{6.7h–k}$$

Note that B_2, E_1 and E_2 are rendered dimensionless by B_1.

We can introduce the stream function of the outer streaming flow ψ by the relations

$$\frac{\partial\psi}{\partial R} = -v_\theta R\sin\theta, \quad \frac{\partial\psi}{\partial\theta} = v_R R^2\sin\theta. \tag{6.8a,b}$$

Using the appropriate harmonics from (5.3) and (5.4), we find from (6.8) the stream functions ψ_1 and ψ_2 in liquids 1 and 2, respectively:

$$\bar{\psi}_1 = \frac{\bar{A}_1}{14}\sin^2\theta\cos\theta(\bar{R}^5 - \bar{R}^3) - \frac{\bar{C}_1}{44}(7\cos^5\theta - 10\cos^3\theta + 3\cos\theta)(\bar{R}^7 - \bar{R}^5), \tag{6.9a}$$

$$\bar{\psi}_2 = \frac{\bar{A}_2}{4}\sin^2\theta\cos\theta\left(1 - \frac{1}{\bar{R}^2}\right) - \frac{5\bar{C}_2}{112}(7\cos^5\theta - 10\cos^3\theta + 3\cos\theta)\left(\frac{1}{\bar{R}^2} - \frac{1}{\bar{R}^4}\right). \tag{6.9b}$$

The stream functions and the radial coordinate R are rendered dimensionless respectively by $B_1^2a^2/(\omega a)$ and by a, and the dimensionless coefficients involved in (6.9) are given by

$$\bar{A}_1 = \bar{\alpha}_{11} - 2\bar{\alpha}_{12}, \quad \bar{C}_1 = -\tfrac{22}{7}(2\bar{\alpha}_{11} + 3\bar{\alpha}_{12}), \tag{6.10a,b}$$

$$\bar{A}_2 = \tfrac{2}{7}(\bar{\alpha}_{21} - 2\bar{\alpha}_{22}), \quad \bar{C}_2 = -\tfrac{8}{5}(2\bar{\alpha}_{21} + 3\bar{\alpha}_{22}). \tag{6.10c,d}$$

The velocities $\bar{\alpha}_{i1}$ and $\bar{\alpha}_{i2}$ entering (6.10) have already been found from (6.7*h–k*). Therefore expressions (6.9) and (6.10) allow graphical representation of the streamlines both inside and outside the drop.

7. Particular cases of the flow fields generated by the oscillating droplet

If liquid outside the droplet is inviscid, $\mu_2 = 0$, then by (6.7*c–e*) $\bar{E}_1 = 0$ and $\bar{E}_2 = -5/3$. Therefore by (6.7*f*, *g*) $K' = -1275/4$, and $K'' = -50$. We also obtain $\bar{\alpha}_{21} = -25/4$ and thus $\bar{\alpha}_{11} = 0$. Also $\bar{\alpha}_{12} = 0$. Thus we obtain in this particular case $\overline{u'_{int}} = \overline{u''_{int}} = \overline{u_{int}} = 0$.

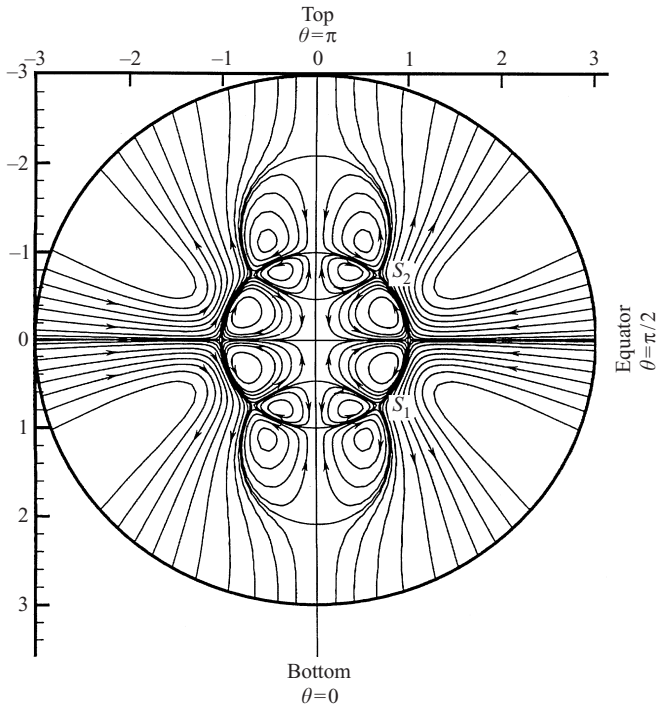

FIGURE 2. Steamlines of the d.c. secondary flow in the case $\rho_1 = \rho_2 = 1\,\mathrm{g\,cm^{-3}}$, $\mu_1 = \mu_2 = 0.01\,\mathrm{g\,cm^{-1}\,s^{-1}}$, $\sigma = 70\,\mathrm{g\,s^{-2}}$, and $a = 0.71\,\mathrm{cm}$. In this case $\omega = 30.64\,\mathrm{s^{-1}}$, $\bar{\alpha}_{11} = 12.96$, $\bar{\alpha}_{12} = -2.21$, $\bar{\alpha}_{21} = 12.96$ and $\bar{\alpha}_{22} = -2.21$. Also $\overline{u'_{int}} = 14.52$, $\overline{u''_{int}} = 0.92$ and $\cos\theta_S = 0.697$.

Consider also the case where $\mu_1 = \mu_2$ and $\rho_1 = \rho_2$. Here $\bar{E}_1 = \bar{E}_2 = -5/6$ and thus

$$K' = \frac{175}{8}\left(\frac{\rho_1 \omega a^2}{2\mu_1}\right)^{1/2}, \quad K'' = 0. \tag{7.1a,b}$$

Taking $\rho_1 = 1\,\mathrm{g\,cm^{-3}}$, $a = 0.71\,\mathrm{cm}$, $\omega = 30.64\,\mathrm{s^{-1}}$ and $\mu_1 = 10^{-2}\,\mathrm{g\,cm^{-1}\,s^{-1}}$ and using (7.1) and the expressions for α_{ij} and $\overline{u'_{int}}$ and $\overline{u''_{int}}$ from (6.7), we find

$$\overline{u_{int}} = 14.52(2\sin\theta\cos^3\theta - \sin\theta\cos\theta) + 0.92(3\sin\theta\cos^3\theta - \sin\theta\cos\theta), \tag{7.2}$$

In another particular case, where $\mu_2 = \infty$, we obtain $\bar{E}_1 = -5/3$, $\bar{E}_2 = 0$, $K' = -300$, $K'' = -1175/2$, $\bar{\alpha}_{21} = 0$, $\bar{\alpha}_{12} = -25/2$, and $\overline{u'_{int}} = \overline{u''_{int}} = \overline{u_{int}} = 0$.

Let us demonstrate the velocity fields of the stationary streaming flow. In figure 2 the streamlines calculated using the expressions (6.9) are shown for the case $\rho_1 = \rho_2 = 1\,\mathrm{g\,cm^{-3}}$, $\mu_1 = \mu_2 = 0.01\,\mathrm{g\,cm^{-1}\,s^{-1}}$, $\sigma = 70\,\mathrm{g\,s^{-2}}$, and $a = 0.71\,\mathrm{cm}$. In this case the interfacial velocity is given by (7.2). The droplet spans the domain $0 \leqslant \bar{R} \leqslant 1$, whereas the outer liquid is shown, as an example, in the domain $1 \leqslant \bar{R} \leqslant 3$. The flow inside the droplet consists, in the present case of $n = 2$, of four toroidal vortices. The stagnation points of the d.c. streaming flow at the droplet surface appear at the bottom ($\theta = 0$), equator ($\theta = \pi/2$) and top ($\theta = \pi$), as well as at the middle points S_1 and S_2 corresponding to

$$\cos^2\theta_S = \frac{\overline{u'_{int}} + \overline{u''_{int}}}{2\overline{u'_{int}} + 3\overline{u''_{int}}} \tag{7.3}$$

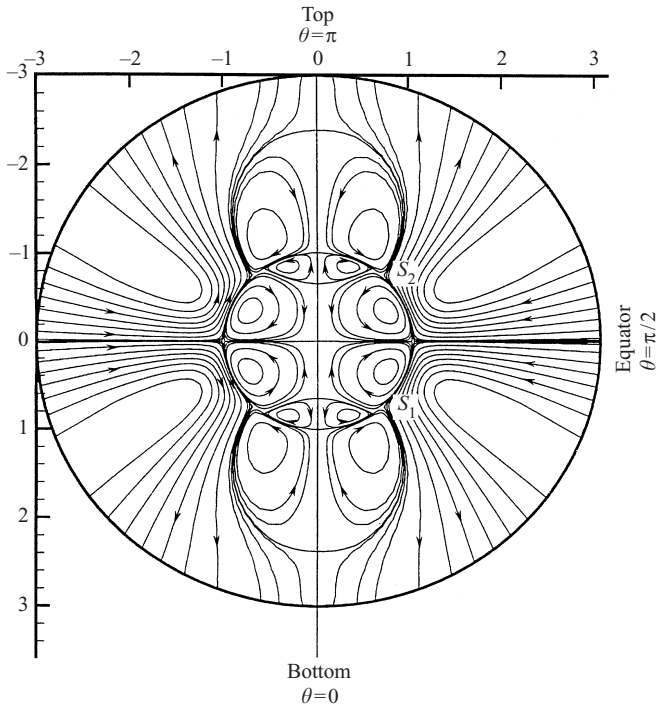

FIGURE 3. As figure 2 but for $\mu_1 = 0.01\,\mathrm{g\,cm^{-1}\,s^{-1}}$, $\mu_2 = 0.02\,\mathrm{g\,cm^{-1}\,s^{-1}}$. In this case $\omega = 30.64\,\mathrm{s^{-1}}$, $\bar{\alpha}_{11} = 9.41$, $\bar{\alpha}_{12} = -3.15$, $\bar{\alpha}_{21} = 10.48$, and $\bar{\alpha}_{22} = -1.01$. Also $\overline{u'_{int}} = 11.55$ and $\overline{u''_{int}} = 1.14$.

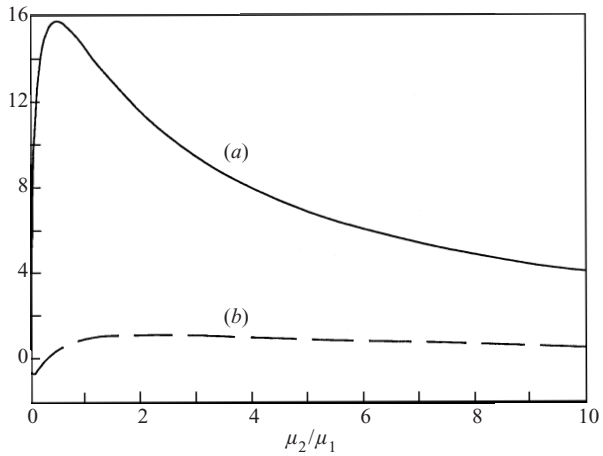

FIGURE 4. Effect of the viscosity ratio μ_2/μ_1 on the interfacial velocity. In this case $\rho_1 = \rho_2 = 1\,\mathrm{g\,cm^{-3}}$, $\mu_1 = 0.01\,\mathrm{g\,cm^{-1}\,s^{-1}}$, μ_2 is variable, $\sigma = 70\,\mathrm{g\,s^{-2}}$, and $a = 0.71\,\mathrm{cm}$. Curve (*a*) $\overline{u'_{int}}$, (*b*) $\overline{u''_{int}}$.

A similar flow pattern for the case $\rho_1 = \rho_2 = 1\,\mathrm{g\,cm^{-3}}$, $\mu_1 = 0.01\,\mathrm{g\,cm^{-1}\,s^{-1}}$, $\mu_2 = 0.02\,\mathrm{g\,cm^{-1}\,s^{-1}}$, $\sigma = 70\,\mathrm{g\,s^{-2}}$, and $a = 0.71\,\mathrm{cm}$ is shown in figure 3.

Figures 4, 5 and 6 show the effect of the ratios μ_2/μ_1, ρ_2/ρ_1, and of the interfacial tension coefficient σ, respectively, on the values of $\overline{u'_{int}}$ and $\overline{u''_{int}}$ characterizing the magnitude of the interfacial velocity $\overline{u_{int}}$.

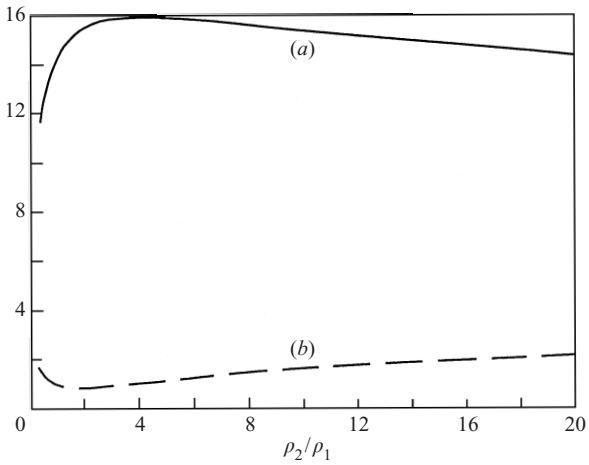

FIGURE 5. Effect of the density ratio ρ_2/ρ_1 on the interfacial velocity. In this case $\rho_1 = 1\,\mathrm{g\,cm^{-3}}$, ρ_2 is variable, $\mu_1 = \mu_2 = 0.01\,\mathrm{g\,cm^{-1}\,s^{-1}}$, $\sigma = 70\,\mathrm{g\,s^{-2}}$, and $a = 0.71\,\mathrm{cm}$. Curve (*a*) $\overline{u'_{int}}$, (*b*) $\overline{u''_{int}}$.

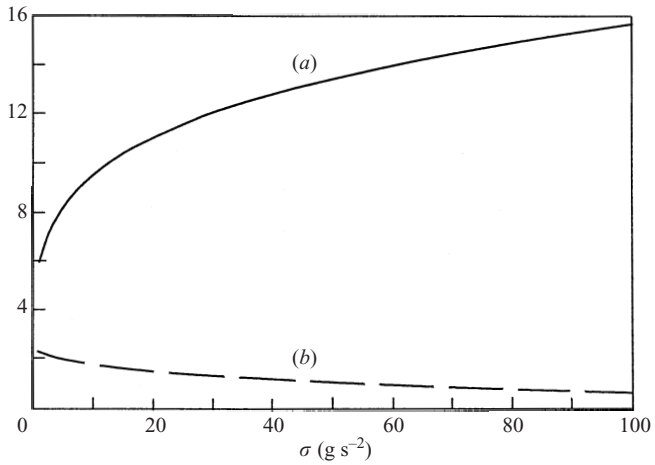

FIGURE 6. Effect of the interfacial tension σ on the interfacial velocity. In this case $\rho_1 = \rho_2 = 1\,\mathrm{g\,cm^{-3}}$, $\mu_1 = \mu_2 = 0.01\,\mathrm{g\,cm^{-1}\,s^{-1}}$, and $a = 0.71\,\mathrm{cm}$. Curve (*a*) $\overline{u'_{int}}$, (*b*) $\overline{u''_{int}}$.

The question arises of what will an experimentalist observe when visualizing flows generated by oscillating droplets. The primary motion in this case, corresponding to the one discussed in Lamb (1959, paragraph 275) and leading to the spectrum (2.3), is given by the stream function

$$\Psi = \left[\sin\omega t \frac{\zeta_{0n}\omega a^3}{n(n+1)}\right] \bar{R}^{n+1} \sin\theta \frac{\mathrm{d}}{\mathrm{d}\theta}[P_n(\cos\theta)], \tag{7.4}$$

which yields for $n = 2$

$$\Psi|_{n=2} = \left[-\sin\omega t \frac{\zeta_{0n}\omega a^3}{2}\right] \bar{R}^3 \sin^2\theta\cos\theta \tag{7.5}$$

and for $n = 3$

$$\Psi|_{n=3} = \left[\sin\omega t \frac{\zeta_{0n}\omega a^3}{24}\right] \bar{R}^4 \sin^2\theta(3 - 15\cos^2\theta). \tag{7.6}$$

It is easy to see that liquid particles as well as seeding particles used for visualization will oscillate in such flows near their initial positions along stationary isolines $\bar{R} = \bar{R}(\theta)$ given by

$$\bar{R}^3 \sin^2\theta\cos\theta = \text{const}, \tag{7.7}$$

in the case $n = 2$, and by

$$\bar{R}^4 \sin^2\theta(3 - 15\cos^2\theta) = \text{const} \tag{7.8}$$

in the case $n = 3$ (cf. figures 7*a* and 7*b*). These isolines are strikingly similar to those shown in the photographs of figure 12 in Trinh *et al.* (1982), and figures 12–15(*a*) in Trinh & Wang (1982) for modes $n = 2$ and 3, which may mean that the photographs actually reveal oscillatory motion of the seeding particles along the stationary isolines. Such a motion should have no effect on mass transfer on the average. On the other hand, a special experimental technique is called for to uncover the steady d.c. streaming depicted in figures 2 and 3 above.

8. Mass transfer due to steady streaming in the case of an oscillating droplet in a liquid–liquid system

We begin consideration of the mass transfer of a passive scalar soluble in liquids 1 and 2 through the interface with an estimate of the thickness of the diffusion boundary layer δ_D, given by

$$\delta_D \sim \frac{a}{(B_i a/\mathscr{D}_i)^{1/2}}, \tag{8.1}$$

where $\mathscr{D}_i$ are the respective diffusion coefficients of the scalar in the two liquids. Its ratio to the thickness of the dynamic Stokes layers $\delta_S \sim (2\nu_i/\omega)^{1/2}$ is given by

$$\frac{\delta_D}{\delta_S} \sim \frac{1}{\sqrt{2\varepsilon Sc}}, \tag{8.2}$$

where according to (2.9) $\varepsilon \sim B_i/(a\omega) \sim \zeta_{0n}$, and the Schmidt number $Sc = \nu_i/\mathscr{D}_i$. The physical process we are dealing with here is intended for protein extraction/concentration. The diffusion coefficient $\mathscr{D}_i$ of proteins is extremely small, which is the main reason for the search for ways to enhance the process. The smallness of $\mathscr{D}_i$ results in large values of the Schmidt number. Taking as an estimate $Sc = 1.4 \times 10^3$ and $\varepsilon = 0.04$ (cf. § 2), we obtain from (8.2) $\delta_D/\delta_S \approx 0.094$. Therefore the diffusion boundary layers is situated at the bottoms of the Stokes layers near the interface. Since the assumption that $\delta_D \ll \delta_S$ approximately holds, we only need the velocity of the stationary streaming very close to the interface to calculate the mass transfer rate of a passive scalar through the interface.

Denote the concentration of the scalar in liquids 1 and 2 by c, with a dimensionality $\mathrm{g\,cm^{-3}}$. Initially we consider both liquids simultaneously, dispensing with the subscripts (or superscripts) i. The diffusion equation reads

$$\frac{\partial c}{\partial t} + u_b\frac{\partial c}{\partial x} + v_b\frac{\partial c}{\partial y} = \mathscr{D}\frac{\partial^2 c}{\partial y^2}, \tag{8.3}$$

where subscript b denotes the velocity components in the vicinity of the interface, close to the bottom of the Stokes layers (cf. (8.4) and (8.7) below).

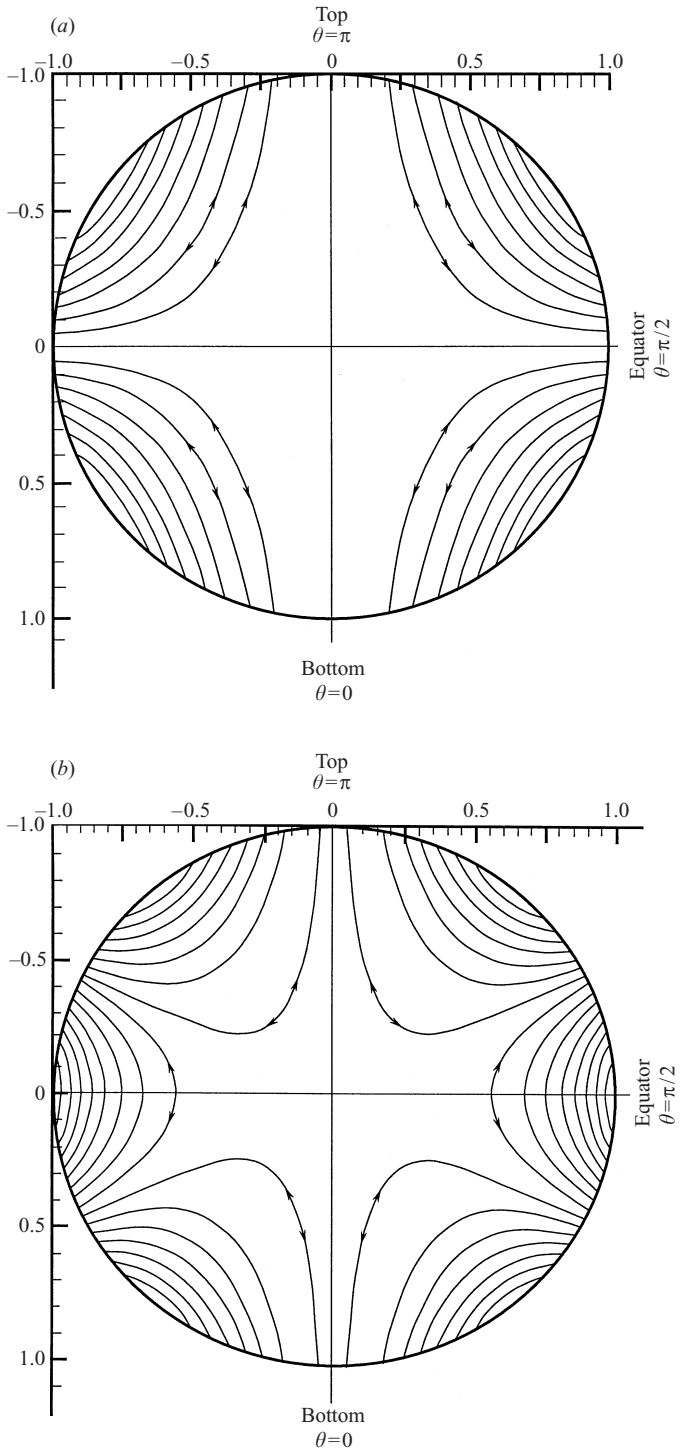

FIGURE 7. The stationary isolines, over which particles oscillate in the primary flow. (*a*) $n = 2$, (*b*) $n = 3$.

As has been mentioned before, for the small diffusion coefficient characteristic of proteins the mass transfer processes take place not over the whole thickness of the dynamic boundary layer, but only close to the interface. In this region the velocity is practically the same as at the interface, which is accounted for in equation (8.3). On the other hand, Mei & Chian (1994), Mei, Fan & Jin (1997), and Mei, Chian & Ye (1998) considered the case of the Schmidt number of order one (cf. (2.11) in Mei & Chian 1994). This means that the thicknesses of the dynamic and diffusion boundary layers were of the same order of magnitude, and the whole flow field affected the mass transfer processes. The assumption (2.11) in Mei & Chian (1994) has been explicitly used to arrive at equation (2.4′) in that work, which was the basis for the whole multiple-scale procedure leading to equation (2.29) there. That equation, indeed, shows that an average of the variation of the flow field inside the whole boundary layer affects transport of the fine particles considered in that work. This however, is only due to the assumption that the kinematic viscosity ν and the diffusion coefficient $\mathscr{D}$ are of the same order of magnitude (which is a plausible approximation for the turbulent flows considered in the above-mentioned works). The physical situation in the present work is totally different. In laminar flows of protein solutions $\mathscr{D} \ll \nu$, and thus, equation (8.3) differs from (2.29) of Mei & Chian (1994) and from (5.21) or (5.22) of Mei *et al.* (1998).

The velocity components u_b and v_b are given by

$$u_b = u_b^{(0)} + u_b^{(1)}, \quad v_b = v_b^{(0)} + v_b^{(1)}, \tag{8.4a,b}$$

where $u_b^{(0)}$ and $v_b^{(0)}$ are given by (4.3) at $\eta = 0$, and $u_b^{(1)} = u_1^{(1)}$ as $\eta \to -0$ or $u_2^{(1)}$ as $\eta \to +0$, $v_b^{(1)} = v_1^{(1)}$ as $\eta \to -0$ or $v_2^{(1)}$ as $\eta \to +0$.

We split the concentration into steady (c_s) and unsteady, variable (c_u) parts

$$c = c_s + c_u. \tag{8.5}$$

It may be shown (for example, cf. Yarin *et al.* 1999) that the time-average mass transfer depends only on c_s, and the diffusion problem reduces to the following equation:

$$\langle u_{b,i}^{(1)} \rangle \frac{\partial c_{s,i}}{\partial x} + \langle v_{b,i}^{(1)} \rangle \frac{\partial c_{s,i}}{\partial y} = \mathscr{D}_i \frac{\partial^2 c_{s,i}}{\partial y^2}, \tag{8.6}$$

where according to (4.8*b*) and (4.7*b*)

$$\langle u_{b,i}^{(1)} \rangle = \tilde{U} \frac{\mathrm{d}\tilde{U}}{\mathrm{d}x} \frac{E_i^2}{4\omega} + \left(\tilde{U} \frac{\mathrm{d}\tilde{U}}{\mathrm{d}x} + \frac{\tilde{U}^2}{r} \frac{\mathrm{d}r}{\mathrm{d}x} \right) \frac{E_i^2}{2\omega} + \alpha_i, \tag{8.7a}$$

$$\begin{aligned} \langle v_{b,i}^{(1)} \rangle = -\frac{1}{r} \frac{\partial \langle u_{b,i}^{(1)} \rangle r}{\partial x} y = -\Bigg\{ & \left[\frac{\mathrm{d}}{\mathrm{d}x} \left(\tilde{U} \frac{\mathrm{d}\tilde{U}}{\mathrm{d}x} \right) + \frac{1}{r} \frac{\mathrm{d}r}{\mathrm{d}x} \tilde{U} \frac{\mathrm{d}\tilde{U}}{\mathrm{d}x} \right] \frac{E_i^2}{4\omega} \\ & + \left[\frac{\mathrm{d}}{\mathrm{d}x} \left(\tilde{U} \frac{\mathrm{d}\tilde{U}}{\mathrm{d}x} + \frac{\tilde{U}^2}{r} \frac{\mathrm{d}r}{\mathrm{d}x} \right) + \frac{1}{r} \frac{\mathrm{d}r}{\mathrm{d}x} \left(\tilde{U} \frac{\mathrm{d}\tilde{U}}{\mathrm{d}x} + \frac{\tilde{U}^2}{r} \frac{\mathrm{d}r}{\mathrm{d}x} \right) \right] \frac{E_i^2}{2\omega} \\ & + \left(\frac{\mathrm{d}\alpha_i}{\mathrm{d}x} + \frac{1}{r} \frac{\mathrm{d}r}{\mathrm{d}x} \alpha_i \right) \Bigg\} y. \end{aligned} \tag{8.7b}$$

Equation (8.6) can be rewritten in the form

$$\frac{\partial^2 c_{s,i}}{\partial y^2} + P_i(x) y \frac{\partial c_{s,i}}{\partial y} = Q_i(x) \frac{\partial c_{s,i}}{\partial x}, \tag{8.8}$$

where

$$P_i(x) = \frac{1}{r}\frac{\partial \langle u_{b,i}^{(1)} \rangle r}{\partial x}\frac{1}{\mathscr{D}_i}, \quad Q_i(x) = \frac{1}{\mathscr{D}_i} q_i(x), \quad q_i(x) = \langle u_{b,i}^{(1)} \rangle. \tag{8.9a–c}$$

The solution for the concentration $c_{s,i}$ is subject to the following boundary conditions:

$$y \to -\infty: \quad c_{s,1} = c_{s\infty,1}, \tag{8.10a}$$

$$y \to +\infty: \quad c_{s,2} = c_{s\infty,2}, \tag{8.10b}$$

$$y = 0: \quad -\mathscr{D}_1 \frac{\partial c_{s,1}}{\partial y} = -\mathscr{D}_2 \frac{\partial c_{s,2}}{\partial y}, \quad c_{s,1} = c_{s,2}. \tag{8.10c}$$

The boundary conditions (8.10a, b) assume that the bulk is well-mixed. This assumption is supported by the results of Baier *et al.* (1999).

The solution of (8.8)–(8.10) is given by (cf. Yarin *et al.* 1999)

$$c_{s,1} = \frac{c_{s\infty,1} + \kappa c_{s\infty,2}}{1+\kappa} - \frac{\kappa(c_{s\infty,1} - c_{s\infty,2})}{1+\kappa} \operatorname{erf}(Z/2), \tag{8.11a}$$

$$c_{s,2} = \frac{c_{s\infty,1} + \kappa c_{s\infty,2}}{1+\kappa} - \frac{(c_{s\infty,1} - c_{s\infty,2})}{1+\kappa} \operatorname{erf}(Z/2), \tag{8.11b}$$

where

$$\kappa = (\mathscr{D}_2/\mathscr{D}_1)^{1/2}, \tag{8.12a}$$

$$Z = y\left[\left|\int_{x_{st}}^{x} \frac{\exp(W(\xi) - W(x))}{Q_i(\xi)}\,\mathrm{d}\xi\right|\right]^{-1/2}, \tag{8.12b}$$

$$W(x) = 2\int_{\text{const}}^{x} \frac{P_i(\xi)}{Q_i(\xi)}\,\mathrm{d}\xi. \tag{8.12c}$$

Note that $W(x)$ is independent of i, in spite of the fact that P_i and Q_i depend on it (cf. (8.9a, b)). The coordinate of a stagnation point is denoted x_{st}. As the lower limit in the integral in Z (cf. (8.12b)), we take the stagnation point of the streaming flow corresponding to the droplet equator $\theta = \pi/2$. Considering mode $n = 2$ and using (5.2), (6.3a), (8.7) and (8.9), we find the following expressions for the mass flux of the admixture at the interface:

$$\langle j_1 \rangle|_{y=0} = \langle j_2 \rangle|_{y=0} = \frac{\sqrt{\mathscr{D}_2}(c_{s\infty,1} - c_{s\infty,2})}{1+\kappa}\, 2\left(\frac{12}{\pi a}\right)^{1/2} I\left(\frac{B_1^2}{\omega a}\right)^{1/2} f(\theta). \tag{8.13}$$

Here $\langle j_1 \rangle|_{y=0} = \langle -\mathscr{D}_i\, \partial c_i/\partial y \rangle|_{y=0}$, and $f(\theta)$ is given by (8.16b) below.

Denote the time-average mass transfer coefficient $\langle h_m \rangle$ and the Sherwood number $\langle Sh \rangle$. Then

$$\langle h_m \rangle (c_{s\infty,1} - c_{s\infty,2}) = \langle j_i \rangle|_{y=0}, \tag{8.14a}$$

$$\langle Sh \rangle = \frac{\langle h_m \rangle a}{\mathscr{D}_1}. \tag{8.14b}$$

Space averaging is given in the present case as

$$\overline{\langle Sh \rangle} = \int_0^l \langle Sh \rangle r\,\mathrm{d}x \Big/ \int_0^l r\,\mathrm{d}x, \tag{8.15}$$

where l is half the perimeter of the droplet cross-section. Using (8.13)–(8.15) we obtain

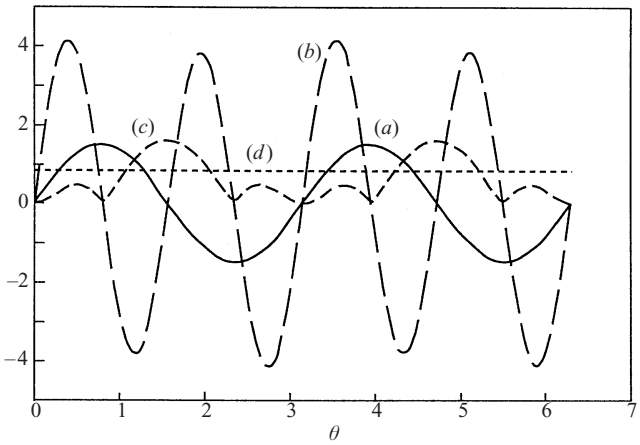

FIGURE 8. Distributions of the parameters relevant for mass transfer due to d.c. streaming generated by droplet oscillations in mode $n = 2$. Curve (*a*) shows the magnitude of the normalized tangential velocity of the primary flow, (*b*) the interfacial velocity of the streaming flow, (*c*) the normalized local Sherwood number, and (*d*) its space-average value. The values of the parameters correspond to those of figure 2.

the local time-average Sherwood number as

$$\langle Sh\rangle = \frac{\kappa}{1+\kappa}\,2\left(\frac{12}{\pi}\right)^{1/2} f(\theta)\frac{|B_1|}{(\omega\mathscr{D}_1)^{1/2}}, \tag{8.16a}$$

$$f(\theta) = \frac{|\sin^2\theta\cos\theta[\overline{u'_{int}}(2\cos^2\theta-1)+\overline{u''_{int}}(3\cos^2\theta-1)]|}{[2(2\overline{u'_{int}}+3\overline{u''_{int}})(1-\sin^6\theta)+3(\overline{u'_{int}}+2\overline{u''_{int}})(\sin^4\theta-1)]^{1/2}}, \tag{8.16b}$$

and the space-average as

$$\overline{\langle Sh\rangle} = \frac{\kappa}{1+\kappa}\,2\left(\frac{12}{\pi}\right)^{1/2}\bar{f}\,\frac{|B_1|}{(\omega\mathscr{D}_1)^{1/2}}, \tag{8.17a}$$

$$\bar{f} = \int_0^{\pi/2} f_1(\theta_1)\,\mathrm{d}\theta_1, \tag{8.17b}$$

$$f_1(\theta_1) = \frac{\cos^3\theta_1\sin\theta_1|[\overline{u'_{int}}(2\sin^2\theta_1-1)+\overline{u''_{int}}(3\sin^2\theta_1-1)]|}{[2(2\overline{u'_{int}}+3\overline{u''_{int}})(1-\cos^6\theta_1)+3(\overline{u'_{int}}+2\overline{u''_{int}})(\cos^4\theta_1-1)]^{1/2}}. \tag{8.17c}$$

As θ tends to $\pi/2$ or θ_1 to 0, both $f(\theta)$ in (8.16*b*) and $f_1(\theta_1)$ in (8.17*c*) tend to the same limit $[(\overline{u'_{int}}+\overline{u''_{int}})/6]^{1/2}$.

Expressions (8.16) show that the local Sherwood number is zero at the bottom and top of the droplet (oscillating in mode $n = 2$) at $\theta = 0$ and π, respectively. Also $\langle Sh\rangle = 0$ at $\theta = \theta_S$ corresponding to the stagnation points S_1 and S_2 (cf. figure 2). On the other hand, at the droplet equator $\theta = \pi/2$, the local Sherwood number reaches its maximum. This is clearly seen in figure 8, where the following curves are plotted: (*a*) the magnitude of the normalized tangential velocity of the primary flow given in the case $n = 2$ by $-\mathrm{d}P_2(\cos\theta)/\mathrm{d}\theta = 3\sin\theta\cos\theta$ according to (2.4) and (2.5*a*); (*b*) $\overline{u_{int}}$ given by (7.2); (*c*) the normalized local Sherwood number $f(\theta)$ according to (8.16); (*d*) its space-average value $\bar{f}$.

Droplet oscillations generate stationary d.c. streaming near the interface which

enhances mass transfer through it. Indeed, expressions (8.16*a*) and (8.17*a*) show that the values of the Sherwood number increased by a factor of the order of $|B_1|/(\omega\mathscr{D}_1)^{1/2} \sim (B_s a/\mathscr{D}_1)^{1/2} \sim (|u_{int}|a/\mathscr{D}_1)^{1/2}$, where $|u_{int}|$ is the magnitude of the interfacial streaming velocity. Taking $|u_{int}| \sim B_s \sim 0.052\,\mathrm{cm\,s^{-1}}$, $a = 0.71\,\mathrm{cm}$ and $\mathscr{D}_1 = 0.71 \times 10^{-5}\,\mathrm{cm^2\,s^{-1}}$, we estimate the factor as 72.

9. Summary and concluding remarks

We can summarize the findings in the present work as follows:

(i) It was shown that standing capillary waves forced at liquid–liquid interfaces lead to significant stationary vortical d.c. flows in the adjoining liquids. Stationary streaming in the Stokes layers near the interface, as well as the corresponding outer streaming (the vortices) in the bulk, were calculated for a liquid droplet immersed in an immiscible liquid.

(ii) It is argued that previous experiments did not reveal the structure of these flows, which however can be traced, for example, by measuring the mass transfer rate of a passive scalar between the adjoining masses of liquids.

(iii) Based on the velocity fields found, the mass transfer equation yielded the mass flux at the interface. It was also shown that it can undergo a drastic increase due to the d.c. secondary vertical flows resulting from the standing waves. The effective diffusion coefficient $\mathscr{D}_{eff}$ appears to be of the order of $\mathscr{D}_1[|u_{int}|\,a/\mathscr{D}_1]^{1/2}$, where $|u_{int}|$ is the magnitude of the interfacial streaming velocity, a is the droplet radius, $\mathscr{D}_1$ the diffusion coefficient in liquid 1 (inside the droplet). The time- and space-average Sherwood numbers $\langle Sh\rangle$, and $\langle\overline{Sh}\rangle$ are of the order of $Sh_0[|u_{int}|\,a/\mathscr{D}_1]^{1/2}$ (Sh_0 being the Sherwood number corresponding to purely diffusional mass transfer), which can easily exceed Sh_0 by two orders of magnitude.

(iv) It is emphasized that the vortical streaming flows lead to enhanced convective transport of the scalar towards the interface, with the resulting steep concentration gradients there. The latter in turn can enhance drastically the mass flux even though the molecular diffusion coefficients $\mathscr{D}_i$ are small.

(v) Similar effects are expected in other flow geometries, for example at the interface between two immiscible planar liquid layers in a narrow channel. Longuet-Higgins (1953) considered several cases of the outer d.c. streaming flow driven by the inner streaming in the Stokes layers due to progressive or standing waves in a single liquid layer. In a series of papers Dore (1970, 1972, 1973) extended the theory for several cases corresponding to the two-layer systems. In all these works the problem considered was purely hydrodynamic (only the streaming flows were calculated). In a separate work to be submitted elsewhere (Yarin 2001) the present author calculated the inter-layer mass transfer rate of a passive scalar in the case of two planar liquid layers in a narrow channel. It has been shown that due to the standing capillary wave at the interface between the layers the enhancement of the effective diffusion coefficient $\mathscr{D}_{eff}$ and the Sherwood numbers $\langle Sh\rangle$ and $\langle\overline{Sh}\rangle$ is described by the above expressions with λ (the wavelength) instead of the droplet radius a.

(vi) Enhancement of the mass flux at liquid–liquid interfaces is of importance in novel bioseparators designed for transferring an admixture from one of the liquids into the other. For example, two-fluid Taylor–Couette flow is an attractive candidate as a key element of novel bioseparator devices, since it is expected that the secondary Taylor vortices will enhance mass transfer of a passive scalar (e.g. a protein) at a liquid–liquid interface (Baier & Graham 1998; Baier *et al.* 1999). Secondary Dean vortices arising in flows in curved (helical) pipes have already found application

in a novel biotechnological module (Gehlert, Luque & Belfort 1998; Kluge *et al.* 1999; Luque *et al.* 1999). In these applications secondary Dean vortices are used to prevent blockage of permeable tubular membranes. However, efforts are also made to generate Dean vortices in two-fluid flows in curved/helical pipes to enhance mass transfer between the phases. A similar effect can also be achieved using natural convection in a horizontal annular pipe with a two-fluid throughflow. However, it is possible to show that significant secondary flows can be achieved only at temperature differences between the inner and outer walls, which might be dangerous for many biomaterials.

In the light of different ideas on novel bioseparators mentioned above, the one considered in the present work possesses an advantage, since it incorporates both an enlarged interfacial area in emulsions of tiny droplets, as well as mass transfer enhancement due to the secondary vortices. Also, in the present case an internal flow inside droplets can be introduced in a controlled manner, which may be beneficial for protein crystal growth (cf. Chung & Trinh 1998). It should be added that secondary vortical flows inside droplets can also be generated using time-periodic electric fields, which also results in mass transfer enhancement (Lee, Im & Kang 2000).

This research was supported in part by BSF – the United States–Israel Binational Foundation, Research Grant No. 97-118. The author acknowledges an anonymous referee who drew his attention to the works of Dore.

REFERENCES

Baier, G. & Graham, M. D. 1998 Two-fluid Taylor-Couette flow experiments and linear theory for immiscible liquids between corrotating cylinders. *Phys. Fluids* **10**, 3045.

Baier, G., Grateful, T. M., Graham, M. D. & Lightfoot, E. N. 1999 Prediction of mass transfer rates in spatially periodic flows. *Chem. Engng Sci.* **54**, 343.

Chung, S. K. & Trinh, E. H. 1998 Containerless protein crystal growth in rotating levitated drops. *J. Cryst. Growth* **194**, 384.

Davidson, B. J. 1971 Mass transfer due to cavitation microstreaming. *J. Sound Vib.* **17**, 261.

Davidson, B. J. 1973 Heat transfer from a vibrating cylinder. *Intl J. Heat Mass Transfer* **16**, 1703.

Dore, B. D. 1970 Mass transport in layered systems. *J. Fluid Mech.* **40**, 113.

Dore, B. D. 1972 A study of mass transport in boundary layers at oscillating free surfaces and interfaces. *Proc. IUTAM Symp. on Unsteady Boundary Layers* (Vol. II, pp. 1535–1583), Laval Univ., Quebec (May 1971). Laval University Press.

Dore, B. D. 1973 On mass transport induced by interfacial oscillations at a single frequency. *Proc. Camb. Phil. Soc.* **74**, 333.

Gehlert, G., Luque, S. & Belfort, G. 1998 Comparison of ultra- and microfiltration in the presence and absence of secondary flow with polysaccharides, proteins, and yeast suspensions. *Biotechnol. Prog.* **14**, 931.

Gopinath, A. & Mills, A. F. 1993 Convective heat transfer from a sphere due to acoustic streaming. *Trans. ASME: J. Heat Transfer* **115**, 333.

Kawahara, N., Yarin, A. L., Brenn, G., Kastner, O. & Durst, F. 2000 Effect of acoustic streaming on the mass transfer from a sublimating sphere. *Phys. Fluids* **12**, 912.

Kluge, T., Rezende, C., Wood, D. & Belfort, G. 1999 Protein transmission during Dean vortex microfiltration of yeast suspensions. *Biotech. Bioengng* **65**, 649.

Lamb, H. 1959 *Hydrodynamics.* Cambridge University Press.

Lee, S. M., Im, D. J. & Kang, I. S. 2000 Circulating flows inside a drop under time-periodic nonuniform electric fields. *Phys. Fluids* **12**, 1899.

Levich, V. G. 1962 *Physicochemical Hydrodynamics.* Prentice-Hall.

Longuet-Higgins, M. S. 1953 Mass transport in water waves. *Phil. Trans. R. Soc. Lond.* A **245**, 535.

Longuet-Higgins, M. S. 1998 Viscous streaming from an oscillating spherical bubble. *Proc. R. Soc. Lond.* A **454**, 725.

Luque, S., Mallubhotla, H., Gehlert, G., Kuriyel, R., Dzengeleski, S., Pearl, S. & Belfort, G. 1999 A new coiled hollow-fiber module design for enhanced microfiltration performance in biotechnology. *Biotech. Bioengng* **65**, 247.

Mei, C. C. 1989 *The Applied Dynamics of Ocean Surface Waves.* World Scientific.

Mei, C. C. & Chian, C. 1994 Dispersion of small suspended particles in a wave boundary layer. *J. Phys. Oceanogr.* **24**, 2479.

Mei, C. C., Chian, C. & Ye, F. 1998 Transport and resuspension of fine particles in a tidal boundary layer near a small peninsula. *J. Phys. Oceanogr.* **28**, 2313.

Mei, C. C., Fan, S. J. & Jin, K. R. 1997 Resuspension and transport of fine sediments by waves. *J. Geophys. Res.* **102**, 15 807.

Rayleigh, Lord 1883 On the circulation of air observed in Kundt's tubes and on some allied acoustical problems. *Phil. Trans. R. Soc. Lond.* **175**, 1.

Rayleigh, Lord 1945 *Theory of Sound.* Dover.

Riley, N. 1997 Acoustic streaming. In *Encyclopedia of Acoustics* (ed. M. J. Crocker), vol. 1, p. 321. Wiley.

Rosenbluth, M. N., Berk, H. L., Doxas, I. & Horton, W. 1987 Effective diffusion in laminar convective flows. *Phys. Fluids* **30**, 2636.

Schlichting, H. 1932 Berechnung ebener periodischer Grenzschichtströmungen. *Phys. Z.* **33**, 327.

Schlichting, H. 1979 *Boundary Layer Theory.* McGraw-Hill.

Trinh, E. H. & Robey, J. L. 1994 Experimental study of streaming flows associated with ultrasonic levitators. *Phys. Fluids* **6**, 3367.

Trinh, E. & Wang, T. G. 1982 Large-amplitude free and driven drop-shape oscillations: experimental observations. *J. Fluid Mech.* **122**, 315.

Trinh, E., Zwern, A. & Wang, T. 1982 An experimental study of small-amplitude drop oscillations in immiscible liquid systems. *J. Fluid Mech.* **115**, 453.

Vold, E. L. 1999 Computational simulations of vorticity enhanced diffusion. *Phys. Fluids* **11**, 3353.

Yarin, A. L. 2001 Stationary d.c. streaming due to capillary waves in a two-layer system and its effect on mass transfer at liquid–liquid interface. *Fluid Dyn. Res.* (submitted).

Yarin, A. L., Brenn, G., Kastner, O., Rensink, D. & Tropea, C. 1999 Evaporation of acoustically levitated droplets. *J. Fluid Mech.* **399**, 151.